X-Ray Imaging Measurements of Capsule Implosions Driven by a *Z*-Pinch Dynamic Hohlraum

J. E. Bailey,[1] G. A. Chandler,[1] S. A. Slutz,[1] G. R. Bennett,[2] G. Cooper,[1] J. S. Lash,[1] S. Lazier,[2] R. Lemke,[1] T. J. Nash,[1] D. S. Nielsen,[2] T. C. Moore,[2] C. L. Ruiz,[1] D. G. Schroen,[3] R. Smelser,[2] J. Torres,[1] and R. A. Vesey[1]

[1]*Sandia National Laboratories, Albuquerque, New Mexico 87185-1196*

[2]*Ktech Corporation, Albuquerque, New Mexico*

[3]*Schafer Corporation, Livermore, California 94550*

(Received 15 April 2002; published 13 August 2002)

The radiation and shock generated by impact of an annular tungsten *Z*-pinch plasma on a 10-mm diam 5-mg/cc CH_2 foam are diagnosed with x-ray imaging and power measurements. The radiative shock was virtually unaffected by *Z*-pinch plasma instabilities. The 5-ns-duration ~135-eV radiation field imploded a 2.1-mm-diam CH capsule. The measured radiation temperature, shock radius, and capsule radius agreed well with computer simulations, indicating understanding of the main features of a *Z*-pinch dynamic-hohlraum-driven capsule implosion.

DOI: 10.1103/PhysRevLett.89.095004 PACS numbers: 52.58.Lq, 52.50.Lp, 52.70.La

Indirect drive inertial confinement fusion (ICF) [1] implodes fuel-filled capsules by converting the laser, ion beam, or *Z*-pinch energy into x rays that fill a hohlraum radiation confinement cavity. X-ray absorption and reemission within the hohlraum produces radiation that is much more symmetric than the original driver. The *Z*-pinch dynamic hohlraum (ZPDH) in an indirect-drive concept [2–6] employing a high-atomic-number (Z) annular *Z*-pinch plasma that implodes onto a cylindrical low-density low-Z foam. The *Z*-pinch impact on the foam launches a radiating shock that propagates toward the cylinder axis. This shock is the main radiation source. The high-opacity *Z*-pinch plasma traps the radiation, serving as the hohlraum wall. Efficient x-ray generation may make this an attractive ICF approach [7,8].

In this Letter, we report on the first measurements of both the radiating shock properties and the radiation-driven capsule evolution within a ZPDH. The ZPDH was created using the Sandia National Laboratories's Z facility to accelerate a tungsten *Z*-pinch plasma onto a cylindrical CH_2 foam. Time-resolved x-ray images of self-emission from the radiating shock propagating at $\sim 35\ \mathrm{cm}/\mu\mathrm{sec}$ in the foam showed that it was remarkably uniform both azimuthally and along the height of the ZPDH. This implies that the effect of *Z*-pinch plasma instabilities on the shock is small. This is encouraging because the corrugated structure associated with *Z*-pinch instabilities was expected to imprint on the shock. Furthermore, computer simulations that neglected instabilities agreed well with the measured shock trajectory and the hohlraum radiation temperature. The radius evolution of a 2.1-mm-diam 60-μm-wall CH capsule, in response to the 135-eV hohlraum radiation, also agreed well with computer simulations. The capsule absorbed more than 10 kJ and reached a radial convergence of approximately five, prior to the impact of the shock. The self-consistent diagnosis of the ZPDH radiation and the resulting capsule implosion proves that ZPDH implosion experiments are feasible and provides a basis for designing experiments aimed at producing x-ray and neutron measurements of the implosion core.

Diagnosing the energetics, hydrodynamics, and symmetry within the hohlraum interior is an overarching challenge for the ZPDH approach to ICF. Radiation-driven capsule implosions should be complete prior to the shock arrival at the axis, since the shock may destroy the implosion symmetry. The radiation ''dwell time'' prior to shock impact is controlled by the ZPDH design. Larger-diameter lower-density foams provide longer dwell times but lower radiation temperatures. Previous experiments [8] exceeded 180 eV temperatures by using a 5-mm-diam, 10-mm-tall, 14 mm/cc foam. The present experiments used a 10-mm-diam, 15-mm-tall, 5 mg/cc foam to increase the dwell time and improve the symmetry, at the expense of lower drive temperature. An important goal was to benchmark simulations to enable reliable optimization of the radiation dwell time and temperature.

Radiation symmetry is a key for ICF. Driving a spherical capsule using a cylindrical dynamic hohlraum is expected to produce an elongated implosion. This can be accounted for [2,4,6] in the experiment design by using a quasispherical ZPDH shape, or by employing radiation baffles within the foam. Random asymmetries generated by plasma instabilities are potentially more insidious. *Z*-pinch plasmas are Rayleigh-Taylor (RT) unstable [5], which could lead to nonuniform radiation generation and production of low opacity regions in the confining radiation case.

The present experiments address this issue by providing the first symmetry measurements of the foam shock emission. The end-on imaging diagnostics also measure the azimuthal symmetry of the capsule implosion. Polar symmetry measurements are more difficult since side-viewing diagnostics must observe the capsule through the *Z*-pinch plasma. Our strategy is to provide benchmark data that will enable future design of capsule implosions that reach the high temperatures needed to produce intense core x-ray emission. The core density determined from x-ray

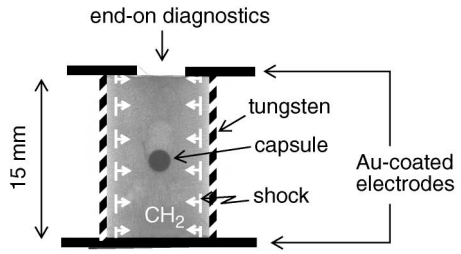

FIG. 1. Dynamic hohlraum schematic diagram. The image of the cylindrically symmetric CH_2 foam and capsule is a preshot x-ray radiograph. The tungsten plasma (striped lines) and foam shock (dashed lines) are illustrations only.

spectroscopy can then be combined with end-on x-ray images to estimate the elongation. Polar symmetry measurements using side-on monochromatic x-ray imaging should also be feasible.

The Z pinch was formed using the 20 MA Z facility [2,9] to accelerate 7.5-μm-diam tungsten wires configured [8,10] in nested arrays with 40- and 20-mm diam and 240 and 120 wires for the outer and inner arrays, respectively (Fig. 1). The principal diagnostics [11] were an eleven-frame time-gated x-ray pinhole camera located at 0° (“end-on”) with respect to the Z-pinch axis and arrays of x-ray diodes (XRD) and bolometers located at 6°. These diagnostics view the dynamic-hohlraum interior through a 5-mm-diam diagnostic aperture. The full width at half maximum for each pinhole frame and the interframe time were ~1.0 ns. The interframe time accuracy was estimated to be ±100 ps and the image timing accuracy with respect to the x-ray power measurements was approximately ±250 ps. The camera is filtered with 4-μm kimfol to record an image dominated mainly by 250 eV photons with ~200 μm spatial resolution.

The time history of the emitted x-ray power was inferred by normalizing the 250 and 500 eV photon energy XRD channels to the bolometers and averaging the result. In other experiments this method was accurate to within ±25% [11,12]. However, the accuracy can vary between experiments, since the source spectrum can change. Nevertheless, the self-consistency of the radiation temperature inferred from the normalization XRD’s and the capsule radius measurements presented below implies that the x-ray power measurements are reasonable.

The Z pinch, shock, and radiation propagating in the foam, and the capsule, can all produce circular features in an end-on x-ray image. To resolve this ambiguity, experiments were conducted using foams with and without an embedded capsule. Representative end-on x-ray images from an empty foam experiment are shown in Fig. 2. The brightness temperature at each time as a function of radius is inferred by normalizing the radial intensity distribution to the measured power and assuming that the radiation source is Planckian. The foam-center temperature rises to ~135 eV (Fig. 3) and remains almost constant for 5.5 ns

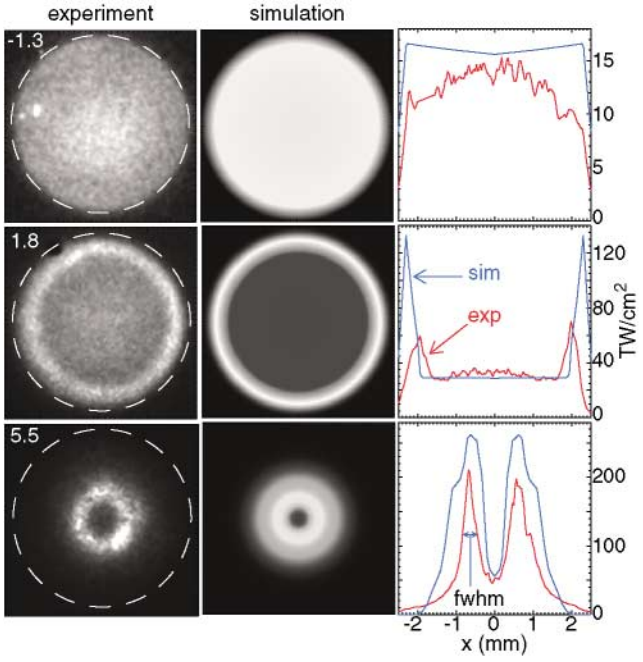

FIG. 2 (color). End-on x ray from an experiment with no embedded capsule. Times given in the upper left corner of each image are in ns with respect to the beginning of the drive radiation plateau (see Fig. 3). The 5-mm-diam diagnostic aperture is shown as a dashed circle. Postprocessed simulation images are shown next to the data. The red curves to the right of each image represent a 200-μm-tall horizontal lineout through the experimental image and the blue curves are corresponding lineouts through the simulation images.

before rising sharply upward as the shock arrives at the foam axis.

The data (Fig. 2) prior to $t = 0$ ns correspond to the period when the radiation has propagated to the center of the foam, but the shock wave and Z-pinch plasma are still

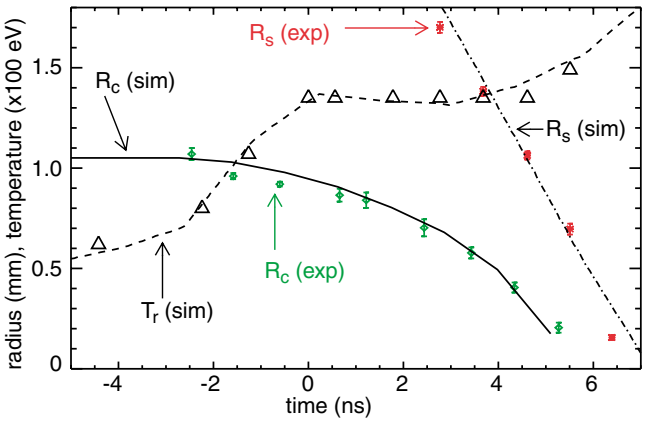

FIG. 3 (color). Time history of the measured radiation temperature at the ZPDH center [T_r (exp); open triangles], the shock radius [R_s (exp); red asterisk with error bars], and the capsule radius [R_c (exp); green diamonds with error bars]. Simulations of the radiation temperature, shock radius, and capsule radius are displayed as dashed, dot-dashed, and solid lines, respectively.

outside the diagnostic aperture. At 0.5 ns an annular emission feature appears and it moves inward in the subsequent frames, reaching the pinch axis at $t = 6.4$–7.1 ns. We have identified this feature as emission from the shock launched in the CH_2 foam, based on two observations. First, the capsule experiments described below demonstrate that when the annular emission feature encounters a capsule located near the foam center, the capsule attenuates the emission by approximately 50%. This implies that the optical depth of the plasma responsible for the annular emission is greater than 7.5 mm. This transparency cannot be associated with the high-opacity tungsten Z-pinch plasma, but is consistent with a shock propagating in the CH_2 foam. Second, one-dimensional (1D) Lagrangian computer simulations using LASNEX [13] predict that the brightest emission arises from the shock and postprocessed simulation images strongly resemble the experiment (Fig. 2). These simulations treat the Z pinch as a smooth, 1-mm-thick, annular plasma. This ignores Rayleigh-Taylor instabilities, an approximation supported by the observations described below. The simulations include radiation losses to the electrodes and appear to reproduce the basic features of the experiment, including the absolute radiation intensity at the foam center, the qualitative observation that the shock emission is a bright annular feature, and the quantitative shock trajectory. We note that the boundary between the tungsten plasma and the shocked foam has not yet been measured, but according to simulations this boundary is located approximately 0.5 mm outside the shock. Also, some discrepancies remain, including the fact that the simulation shock emission width and intensity are both too large. The width discrepancy may indicate that the plasma behind the shock cools faster in the experiment. The excellent overall agreement is evidence for a reasonable level of ZPDH energetics and hydrodynamics understanding.

The shock trajectory was measured by taking lineouts every 18° through each image and measuring the diameter. Throughout most of the pulse the shock velocity was constant at 35 ± 4 cm/μsec, corresponding to a simulation shock pressure of approximately 6 Mbar. The measured annular width of the shock emission was 360 μm$\pm$7%, constant over time to within the measurement accuracy. This width is essentially the same as the convolution of the instrument resolution with the motional blurring due to the time gate duration and the high shock velocity. The true shock emission width was therefore less than approximately 200 μm. The measurements integrate over most of the 15 000-μm height of the foam. Thus, any variation in the shock launch time or shock strength induced by the RT (or any other nonuniformity) is very small. Furthermore, the azimuthal standard deviation of the shock radius is $\pm$1–4%, another indication of good symmetry. The standard deviation of the shock emission intensity is larger, typically $\pm$20–30%. This is probably due to foam density variations, since a variation in the shock strength should appear as a velocity difference. While it is desirable to improve this in future experiments, the radiation intensity at a capsule will be much smoother, due to the low foam opacity and the hohlraum radiation confinement. We consider the small effect of pinch nonuniformities on the shock to be an important breakthrough in the prospects for ZPDH ICF.

End-on x-ray images and representative lineouts from an imploding capsule experiment are shown in Figs. 4 and 5, respectively. The capsule was a 2.1-mm-diam CH shell with a 55.3 μm wall thickness, a 4.5 μm PVA overcoat, and a 12 atm D_2/0.075 atm Ar gas fill. The capsule was embedded within the foam during the casting process, and the capsule positioning was determined prior to the experiment using x-ray radiography. The Fig. 4 images are from a first experiment in which the capsule was inadvertently positioned about 0,5 mm away from the cylindrical axis. Subsequent experiments have demonstrated that improved capsule centering is feasible and this is not considered an impediment to ICF.

The capsule images are a convolution of thermal radiation originating from above and below the capsule with the self-emission from the capsule ablation plasma. The capsule shell absorbs the thermal radiation from below the capsule, forming a self-backlit image of the capsule implosion (Figs. 4 and 5). The observation of capsule

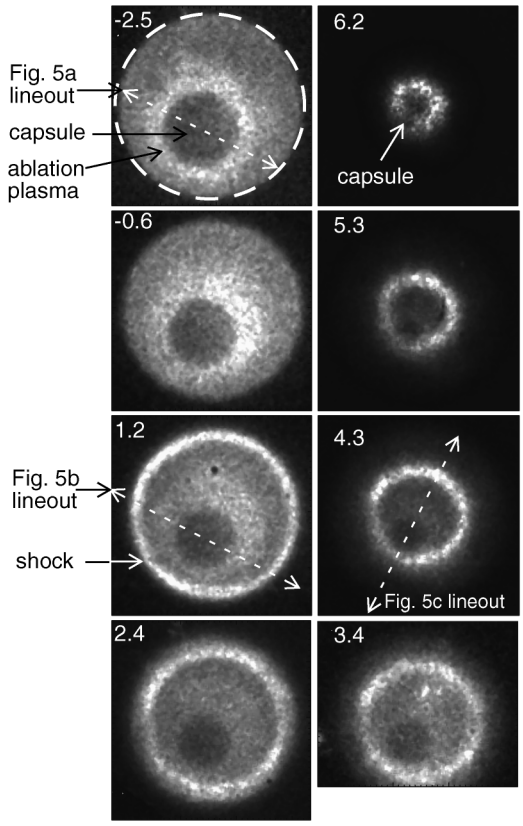

FIG. 4. End-on x-ray images from a capsule implosion experiment. Times given in the upper left corner of each image are in ns. The locations of lineouts displayed in Fig. 5 are shown as dotted arrows.

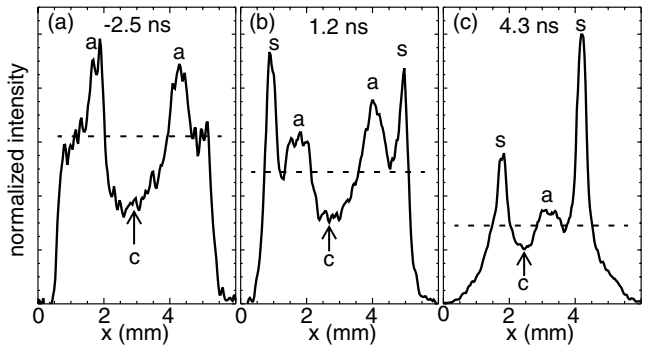

FIG. 5. Capsule implosion experiment lineouts. The time and orientation of lineouts (a), (b), and (c) are indicated in Fig. 4. The feature labels "a", "s", and "c" correspond to the ablation plasma emission, the shock emission, and the capsule absorption, respectively. The dashed horizontal lines represent the approximate intensity of the thermal radiation corresponding to the temperature displayed in Fig. 3.

absorption confirms that the optical depth of the radiation-heated CH_2 plasma is at least 7.5 mm, the depth of the capsule within the foam. The capsule ablation plasma emission appears as a limb-brightened ring around the capsule (Figs. 4 and 5). The initial images consist of thermal radiation, the ablation plasma emission, and the self-absorbed capsule (-2.5 ns, -0.6 ns in Fig. 4; Fig. 5(a)). Subsequently, the shock also appears within the diagnostic aperture. Note the intensity scale in each Fig. 4 frame has been normalized. The shock converges onto the pinch axis as the slightly offaxis capsule implodes. The shock first impacts the capsule between 4.3 and 5.3 ns and at 6.2 ns the shock envelops the capsule. Lineouts through the 6.2 ns image demonstrate that at the capsule location, the shock intensity is reduced by $\sim$50%, a key observation for identification of the shock emission.

The capsule diameter as a function of time was measured from lineouts taken through each image every 18°. The angle averaged diameter was divided by two in order to determine the capsule radius (Fig. 3). The uncertainties include the angular variation and the uncertainty in the image interpretation when the ablation plasma emission, the thermal radiation, and the shock emission begin to compete. The azimuthal standard deviation was $\pm 1\%$ initially (-2.5 ns, -0.6 ns frames, Fig. 4), rising to $\pm 19\%$ as the shock began to impact the capsule (5.3 ns frame, Fig. 4). The capsule absorbed approximately 11 kJ, estimated from the measured temperature and capsule radius evolution and assuming an albedo consistent with simulations of 0.2. The capsule converges by a factor of 5 in the radius-azimuthal angle plane (Fig. 3). However, no neutrons or core-generated x rays were observed.

1D capsule implosion computer simulations [13] were performed to evaluate the self-consistency of the measured radiation and the capsule radius evolution. The Lagrangian simulations used the measured radiation temperature as input and computed the implosion of a spherical capsule embedded in a spherical foam. The calculated capsule radius, obtained by postprocessing the simulations, agreed well with the measurements (Fig. 3). Varying the incident temperature on the capsule by $\pm 10\%$ from the measured value was found to alter the implosion time by approximately 1–1.5 ns. Such a discrepancy would be readily measured, and we therefore conclude that the measurements of the radiation and the capsule implosion are self-consistent. The average simulation fuel temperature was $\sim$500 eV, too low to generate observable neutron or core x-ray signals with existing diagnostics.

The most significant results reported here are the ability to self-consistently diagnose conditions inside a ZPDH and the observation that the shock, the main radiation source for heating the hohlraum, is affected very little by *Z*-pinch nonuniformities. The measurements provide the basis for validating simulations of the ZPDH physics. We are using these benchmarked simulations to design ZPDH driven capsule implosions that will employ a shorter radiation dwell time and a higher radiation temperature to achieve a hot implosion core that emits diagnostic x rays.

We thank the target fabrication group at General Atomics Corporation, the Z target fabrication and materials processing groups, and the Z diagnostics, wire array, and accelerator teams for invaluable and dedicated technical assistance. L. P. Mix helped with image processing and manuscript review. L. Ruggles and W. Simpson provided the preshot radiographs. We are grateful to R. J. Leeper, J. L. Porter, T. A. Mehlhorn, and M. K. Matzen for support and encouragement. Sandia is a multiprogram laboratory operated by Sandia Corporation, a Lockheed Martin Company, for the U.S. Department of Energy under Contract No. DE-AC04-94AL85000.

[1] J. Lindl, Phys. Plasmas **2**, 3933 (1995).
[2] M. K. Matzen, Phys. Plasmas **4**, 1519 (1997); D. D. Ryutov, M. S. Derzon, and M. K. Matzen, Rev. Mod. Phys. **72**, 167 (2000).
[3] V. P. Smirnov, Plasma Phys. Controlled Fusion **33**, 1697 (1991).
[4] J. H. Brownell, R. L. Bowers, K. D. McLenthan, and D. L. Peterson, Phys. Plasmas **5**, 2071 (1998).
[5] D. L. Peterson *et al.*, Phys. Plasmas **6**, 2178 (1999).
[6] S. A. Slutz *et al.*, Phys. Plasmas **8**, 1673 (2001).
[7] J. Lash *et al.*, in *Proceedings of Inertial Fusion Science and Applications 99, Bordeaux, France, 1999*, edited by C. Labaune, W. J. Hogan, and K. A. Tanaka (Elsevier, Paris, 2000), Vol. I, p. 583.
[8] T. J. Nash *et al.*, Phys. Plasmas **6**, 2023 (1999).
[9] R. J. Leeper *et al.*, Nucl. Fusion **39**, 1283 (1999).
[10] T. W. L. Sanford *et al.*, Phys. Plasmas **7**, 4669 (2000).
[11] T. J. Nash *et al.*, Rev. Sci. Instrum. **72**, 1167 (2001).
[12] M. E. Cuneo *et al.*, Phys. Plasmas **8**, 2257 (2001); T. W. L. Sanford *et al.* (to be published).
[13] G. Zimmerman and W. Kruer, Comments Plasma Phys. Control. Fusion, **2**, 85 (1975).